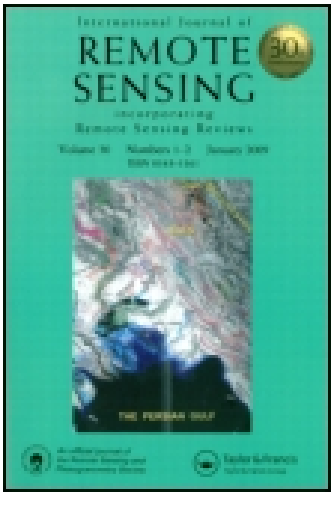

International Journal of Remote Sensing

Publication details, including instructions for authors and subscription information:
http://www.tandfonline.com/loi/tres20

The roles of textural images in improving land-cover classification in the Brazilian Amazon

Dengsheng Lu[ab], Guiying Li[b], Emilio Moran[b], Luciano Dutra[c] & Mateus Batistella[d]

[a] Zhejiang Provincial Key Laboratory of Carbon Cycling in Forest Ecosystems and Carbon Sequestration, School of Environmental & Resource Sciences, Zhejiang A&F University, Hangzhou, Zhejiang Province 311300, China

[b] Center for Global Change and Earth Observations, Michigan State University, East Lansing, MI 48864, USA

[c] National Institute for Space Research, São Jose dos Campos 12245-010, SP, Brazil

[d] Embrapa Satellite Monitoring, Campinas 13088-300, SP, Brazil

Published online: 04 Dec 2014.

To cite this article: Dengsheng Lu, Guiying Li, Emilio Moran, Luciano Dutra & Mateus Batistella (2014) The roles of textural images in improving land-cover classification in the Brazilian Amazon, International Journal of Remote Sensing, 35:24, 8188-8207, DOI: 10.1080/01431161.2014.980920

To link to this article: http://dx.doi.org/10.1080/01431161.2014.980920

International Journal of Remote Sensing, 2014
Vol. 35, No. 24, 8188–8207, http://dx.doi.org/10.1080/01431161.2014.980920

The roles of textural images in improving land-cover classification in the Brazilian Amazon

Dengsheng Lu[a,b]*, Guiying Li[b], Emilio Moran[b], Luciano Dutra[c], and Mateus Batistella[d]

[a]*Zhejiang Provincial Key Laboratory of Carbon Cycling in Forest Ecosystems and Carbon Sequestration, School of Environmental & Resource Sciences, Zhejiang A&F University, Hangzhou, Zhejiang Province 311300, China;* [b]*Center for Global Change and Earth Observations, Michigan State University, East Lansing, MI 48864, USA;* [c]*National Institute for Space Research, São Jose dos Campos 12245-010, SP, Brazil;* [d]*Embrapa Satellite Monitoring, Campinas 13088-300, SP, Brazil*

(*Received 2 June 2014; accepted 23 September 2014*)

Texture has long been recognized as valuable in improving land-cover classification, but how data from different sensors with varying spatial resolutions affect the selection of textural images is poorly understood. This research examines textural images from the Landsat Thematic Mapper (TM), ALOS (Advanced Land Observing Satellite) PALSAR (Phased Array type L-band Synthetic Aperture Radar), the SPOT (Satellite Pour l'Observation de la Terre) high-resolution geometric (HRG) instrument, and the QuickBird satellite, which have pixel sizes of 30, 12.5, 10/5, and 0.6 m, respectively, for land-cover classification in the Brazilian Amazon. GLCM (grey-level co-occurrence matrix)-based texture measures with various sizes of moving windows are used to extract textural images from the aforementioned sensor data. An index based on standard deviations and correlation coefficients is used to identify the best texture combination following separability analysis of land-cover types based on training sample plots. A maximum likelihood classifier is used to conduct the land-cover classification, and the results are evaluated using field survey data. This research shows the importance of textural images in improving land-cover classification, and the importance becomes more significant as the pixel size improved. It is also shown that texture is especially important in the case of the ALOS PALSAR and QuickBird data. Overall, textural images have less capability in distinguishing land-cover types than spectral signatures, especially for Landsat TM imagery, but incorporation of textures into radiometric data is valuable for improving land-cover classification. The classification accuracy can be improved by 5.2–13.4% as the pixel size changes from 30 to 0.6 m.

1. Introduction

Remote-sensing data show land surface features when a spaceborne or airborne craft passes over terrain and are commonly used for mapping land-cover distribution. A land-cover classification from remote-sensing data is a comprehensive procedure that requires careful consideration of different aspects, such as user's needs, complexity of land-cover types, extent of the study area, classification system, selection of remote-sensing variables and corresponding classification algorithms, as well as the analyst's experience and knowledge (Lu and Weng 2007). When one decides to implement a classification, the data sets, study area, and classification system may be already determined, thus one critical step is to select suitable variables for implementing land-cover classification using a proper algorithm. Much previous research has explored

*Corresponding author. Emails: luds@zafu.edu.cn; ludengsh@msu.edu

classification algorithms, from statistics-based (e.g. maximum likelihood, minimum distance) to non-statistics-based algorithms (e.g. neural network, decision tree, *k*-nearest neighbour, support vector machine) and from pixel-based to subpixel-based and object-oriented algorithms (Lu and Weng 2007; Marpu et al. 2012; Yu et al. 2012). Because of the difficulty in identifying the best classification algorithm, a comparative analysis of different classification algorithms is usually conducted for a specific study area (Lu et al. 2004; Li, Lu, Moran, and Sant'Anna 2012).

In addition to development of advanced classification algorithms, another active research topic is the selection of suitable variables. Different sensor data may have various capabilities for land-cover classification. For example, optical sensor data have spectral, spatial, radiometric, and temporal features, and radar data have unique features in polarization options (HH, horizontal transmitted and received polarization; HV, horizontal transmitted and vertical received polarization; VV, vertical transmitted and received polarization; VH, vertical transmitted and horizontal received polarization). When one decides to use specific sensor data such as Landsat for land-cover classification, the radiometric and temporal features are constant, but the spectral and spatial features are the most important features to be further explored. From multispectral bands, one can produce many new variables using image-processing techniques, such as vegetation indices and image transforms (Bannari et al. 1995; McDonald, Gemmell, and Lewis 1998). These techniques are based on individual pixels without incorporation of spatial relationships.

Spatial features reflect the association between nearby pixels; that is, the spatial relationships between one central pixel and its neighbours (Dutra and Mascarenhas 1984). One common method that uses spatial features is through the use of textural images. Texture refers to spatial variation of image tones. There is more homogeneity within the texture than between different textures. In general, a good texture image should have three key components: enhanced features of interesting land surfaces, reduced heterogeneity within the same land-cover type, and preserved clear boundaries between different land-cover types. Of the many textural measures (Li, Lu, et al. 2011; Kourgli et al. 2012; Rodriguez-Galiano et al. 2012; Seetharaman and Palanivel 2013), GLCM (grey-level co-occurrence matrix) (Haralick, Shanmugam, and Dinstein 1973; Marceau et al. 1990) may be the most commonly used method to extract textural images from remotely sensed data, especially from high spatial resolution images such as IKONOS and QuickBird (Herold, Liu, and Clarke 2003; Coburn and Roberts 2004; Wang et al. 2004; Johansen et al. 2007; Agüera, Aguilar, and Aguilar 2008; Su et al. 2008) and even Landsat (Li, Lu, et al. 2011; Wood et al. 2012). Textures have been used for different applications such as land-cover classification (Li, Hayward, et al. 2011; Jin et al. 2012; Rodriguez-Galiano et al. 2012) and estimation of forest attributes such as biomass and tree height (Kuplich, Curran, and Atkinson 2005; Kayitakire, Hamel, and Defourny 2006; Sarker and Nichol 2011; Cutler et al. 2012; Lu et al. 2012; Wood et al. 2012) and biodiversity (e.g. plant species richness, avian species richness) (Culbert et al. 2012; Viedma et al. 2012).

Although textural images have been extensively explored and applied in previous research, how different sensor data with various spatial resolutions affect the selection of textural images and how this affects land-cover classification are poorly understood. The complexity in identifying suitable textures for a specific study makes it difficult to select optimal textural images because it requires one to take texture measures, image bands, moving window sizes, quantization levels, and other factors into account (Chen, Stow, and Gong 2004). No general guidelines to support the selection of an optimal texture are available because of the different spatial patterns and compositions of the land-cover types under investigation. Therefore, textural images are not extensively applied as spectral features in land-cover classification in practice, but they have been regarded as effective ways to improve classification performance if the optimal textural images can be obtained for a specific study. Based on our previous research

in the Brazilian Amazon using data acquired by the Landsat Thematic Mapper (TM), ALOS (Advanced Land Observing Satellite) PALSAR (Phased Array type L-band Synthetic Aperture Radar), the SPOT (Satellite Pour l'Observation de la Terre) high-resolution geometric (HRG) instrument, and the QuickBird satellite (Li, Lu, et al. 2011, Li, Lu, Moran, Dutra, et al. 2012; Lu et al. 2008, 2012), this article provides a comparative analysis of textural images from the aforementioned sensor data to examine how different sensor data with various spatial resolutions affect the selection of textural images. Through this comparative analysis, we can better understand the roles of textural images in improving land-cover classification and how to effectively select suitable textures from different sensor data, which have not been examined in previous research.

2. Study areas

After considering data availability (satellite images and field survey data) and the land-cover classification objectives, three study areas in the Brazilian Amazon – Altamira in Pará State, Machadinho d'Oeste in Rondônia State, and Lucas do Rio Verde in Mato Grosso State – were selected in this research (Figure 1). These areas vary considerably in terms of their land-use

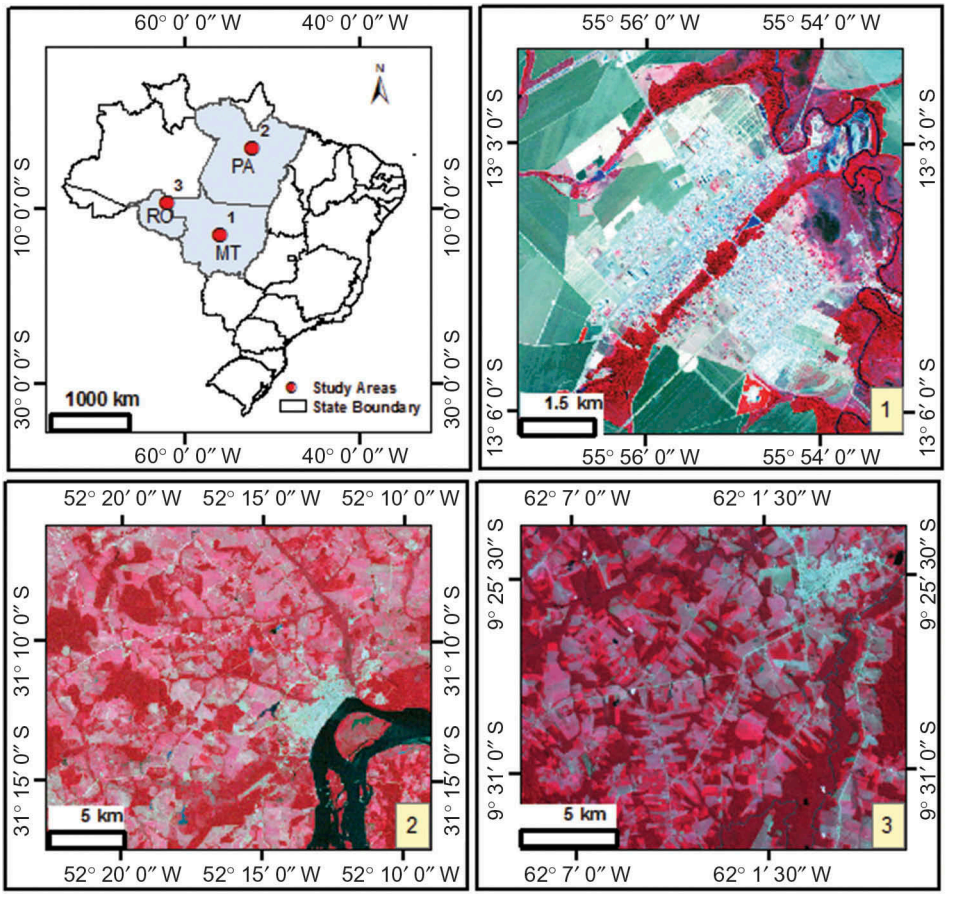

Figure 1. Study areas: (1) Lucas do Rio Verde in Mato Grosso State, shown using a QuickBird image; (2) Altamira in Pará State, shown using a Landsat 5 TM image; and (3) Machadinho d'Oeste in Rondônia State, shown using a SPOT 5 HRG image.

Note: The colour image is a composite of near-infrared, red, and green spectral bands by assigning as red, green, and blue, respectively.

history and complexity of landscapes. Altamira is located along the Transamazon Highway in the northern Brazilian state of Pará. The terrain is undulating with the highest elevation of approximately 350 m in the uplands and the lowest elevation of approximately 10 m in floodplains along the Xingu River. The dominant native vegetation types are mature moist forest and liana forest. Since the early 1970s, deforestation has led to a complex composition of different land-cover types such as successional forest stages, pasture, and agricultural lands. Machadinho d'Oeste is located in the northeast part of Rondônia State in western Brazil. The terrain is undulating with elevation ranging from 100 to 450 m. Major deforestation began here in the late 1980s. Due to land-use intensification, most successional vegetation is in the initial and intermediate stages. In deforested areas, pastures, perennial crops (e.g. coffee, cocoa), agroforestry (e.g. cocoa associated with rubber-producing trees), and small fields of annual crops are common land uses. Lucas do Rio Verde is a relatively small county and yet has complex urban–rural spatial patterns derived from its highly capitalized agricultural base of soybean production, large silos and warehouses, and planned urban growth. The major vegetation includes primary forest, cerrado, and limited areas of plantation and regenerating vegetation. The three study areas provide a range of land-cover conditions, spatial patterns, and types of land use that together make them an ideal set of areas to test the ideas described in this article.

3. Methods

3.1. Data collection and preprocessing

Landsat TM, ALOS PALSAR, SPOT HRG, and QuickBird images with original pixel sizes of 30, 12.5, 10/5, and 0.6 m, respectively, were used for a comparative analysis of land-cover classification in the Brazilian Amazon. The major features of the selected data sets, which included satellite images and field survey data, are summarized in Table 1. The Landsat TM imagery has six spectral bands covering the visible, near infrared (NIR), and shortwave infrared (SWIR) bands with 30 m spatial resolution. This image was radiometrically and atmospherically calibrated using the improved image-based dark object subtraction model (Chavez 1996; Chander, Markham, and Helder 2009). Both Landsat TM and ALOS PALSAR data were used for land-cover classification at Altamira. The 2008 Landsat TM imagery was geometrically registered to a previously corrected Landsat 5 TM image with UTM coordinates (zone 22 south) and the geometric error (i.e. root mean square error, RMSE) was less than 0.5 pixels. The ALOS PALSAR L-band image was then registered to the 2008 Landsat TM image with an RMSE of 1.020 pixels based on 28 control points. The ALOS PALSAR HH and HV images with a pixel size of 12.5 m were resampled to a pixel size of 10 m using the nearest-neighbour technique during the image-to-image registration. Speckle was reduced using the Lee-Sigma filtering algorithm with a window size of 5 × 5 pixels (Li, Lu, et al. 2011).

The SPOT HRG image has five bands covering one panchromatic band with 5 m spatial resolution, two visible (green and red) bands and one NIR band with 10 m spatial resolution, and one SWIR band with 20 m spatial resolution. The HRG image was also atmospherically calibrated by image-based dark object subtraction (Lu et al. 2008). The 20 m SWIR image was resampled to 10 m, the same pixel size as the SPOT visible and NIR images. No geometric rectification for this SPOT image was conducted due to the fact that this image had precise geometric accuracy through comparison with the previously registered Landsat TM imagery.

QuickBird has four multispectral bands with 2.4 m spatial resolution and one panchromatic band with 0.6 m. In order to make full use of its multispectral and panchromatic features, the wavelet-merging technique was used to integrate both multispectral and

Table 1. Data sets used in selected study areas.

Study area	Field survey	Sensor	Major characteristics	Date
Altamira, northern Pará State, Brazil	During July–August 2009, a total of 432 sample plots were collected, including 220 plots for use as training sample plots; the remaining 212 plots were used as test samples	Landsat 5 TM	TM image with 30 m spatial resolution and six spectral bands, covering three visible bands (blue, green, and red), one near-infrared (NIR) band, and two shortwave-infrared (SWIR) bands	2 July 2008
		ALOS PALSAR	ALOS PALSAR FBD (fine beam double polarization) Level 1.5 products with HH and HV polarization options (ground range, unsigned 16 bit integral number, 12.5 m pixel spacing)	2 July 2009
Machadinho d'Oeste in northeastern Rondônia State, Brazil	Fieldwork was conducted in August 2002 and August 2003. More than 200 sample plots (12–20 plots for each land-cover type) were used as training samples, and 306 test samples were used for accuracy assessment	SPOT 5 HRG	HRG image with five spectral bands covering one panchromatic band with spatial resolution of 5 m, two visible (green and red) bands and one NIR band of 10 m, and one SWIR band of 20 m	26 June 2003
Lucas do Rio Verde in Mato Grosso State, Brazil	At least 15 sample plots for each training class were selected, and another 300 test samples were randomly selected, based on visual interpretation of the QuickBird image	QuickBird	Quickbird image has four multispectral bands (blue, green, red, and NIR) with 2.4 m spatial resolution and one panchromatic band (visible wavelength) with 0.6 m spatial resolution. The wavelet-merging technique was used to integrate multispectral and panchromatic data into a new multispectral image with 0.6 m spatial resolution	20 June 2008

panchromatic data into a new fused multispectral image with 0.6 m spatial resolution (Lu, Hetrick, and Moran 2010). Because of its high geometric accuracy, no geometric rectification was needed.

In addition to the satellite images, field survey data for each study area were also collected; part of the data set was used as training samples for land-cover classification, and the remaining samples were used as test samples for evaluation of the classification results. The number of training and test samples used in each study area is also summarized in Table 1.

3.2. *Extraction of textural images*

Figure 2 illustrates the framework for integrating textural images as extra bands into multispectral or radiometric images in order to examine the role of texture in improving land-cover classification accuracy. In this research, the critical step is to identify suitable textures for use in image classification. Therefore, the GLCM-based texture measures are used and the relevant formulae are summarized in Table 2. The methods for extracting textural images from different sensor data (e.g. Landsat TM, ALOS PALSAR, SPOT HRG, and QuickBird) are summarized in Table 3, for which radiometric bands and window sizes are considered for each texture measure. Previous research has indicated that a single texture image is not enough to effectively extract the spatial features; however, a combination of two textural images can provide sufficient capability but adding more textural images does not significantly improve the land-cover classification (Lu et al. 2008; Li, Lu, et al. 2011). Based on the analysis of the training samples using the textural images, separability analysis using the transformed divergence algorithm was used to identify potential combinations of two textural images. Because not all texture combinations were needed, it was necessary to develop a suitable method to make sure that the selected combination provides the richest source of information for land-cover classification (Pathak and Dikshit 2010; Li, Lu, Moran, Dutra, et al. 2012). One simple solution is based on the analysis of standard deviations and correlation coefficients according to Equation (1):

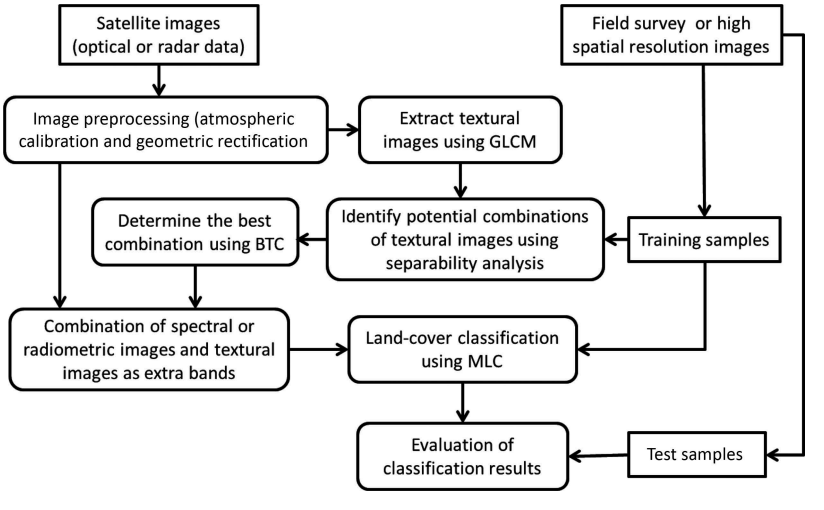

Figure 2. Framework for combining textural images as extra bands into multispectral or radar data for land-cover classification.

Table 2. The GLCM-based texture measures.

No.	Texture measure	Formula
1	Mean (MEA)	$\text{MEA} = \sum_{i,j=0}^{N-1} i(P_{i,j})$
2	Variance (VAR)	$\text{VAR} = \sum_{i,j=0}^{N-1} P_{i,j}(i - \text{MEA})^2$
3	Homogeneity (HOM)	$\text{HOM} = \sum_{i,j=0}^{N-1} \frac{P_{i,j}}{1+(i-j)^2}$
4	Contrast (CON)	$\text{CON} = \sum_{i,j=0}^{N-1} P_{i,j}(i-j)^2$
5	Dissimilarity (DIS)	$\text{DIS} = \sum_{i,j=0}^{N-1} P_{i,j}\lvert i-j\rvert$
6	Entropy (ENT)	$\text{ENT} = \sum_{i,j=0}^{N-1} P_{i,j}(-\ln P_{i,j})$
7	Second moment (SEM)	$\text{SEM} = \sum_{i,j=0}^{N-1} {P_{i,j}}^2$
8	Correlation (COR)	$\text{COR} = \sum_{i,j=0}^{N-1} P_{i,j}\left[\frac{(i-\text{MEA}_i)(j-\text{MEA}_j)}{\sqrt{(\text{VAR}_i)(\text{VAR}_j)}}\right]$

Note: $P_{i,j} = V_{i,j} \Big/ \sum_{i,j=0}^{N-1} V_{i,j}$, where $V_{i,j}$ is the value in the cell (i, j) (row i and column j) of the moving window and N is the number of rows or columns.

$$\text{Best texture combination (BTC)} = \frac{\sum_{i=1}^{n} \text{STD}_i}{\sum_{j=1}^{n} \lvert r_{ij}\rvert}, \tag{1}$$

where STD_i is the standard deviation of the textural image i, r_{ij} is the correlation coefficient between two textural images i and j, and n is the total number of textural images available. A higher BTC value indicates a better combination of textural images (Li, Lu, et al. 2011).

3.3. *Land-cover classification and evaluation*

As shown in Figure 2, the identified best combination of textural images is combined into multispectral (or radiometric for ALOS PALSAR) data as extra bands, and these are then used for land-cover classification. As a comparison, the classification was also conducted for spectral/radiometric data only. Training samples are collected during the fieldwork in different years for each study area. Because use of a maximum likelihood classifier is the most common approach that is both robust and also available in all image-processing software (Lu and Weng 2007), it was used in this research to implement the land-cover classification for the corresponding images. The classification results were evaluated using the test sample plots from the field surveys.

An error matrix is commonly used for assessing land-cover classification results. Overall accuracy, kappa coefficient, and user's and producer's accuracies are then calculated from the error matrix (Congalton 1991; Congalton and Green 2008; Foody 2002, 2009). The

Table 3. Summary of methods used for extracting textural images.

Sensor data	Bands	Texture measures	Window size(s)	Reference
Landsat TM	Green, red, NIR, SWIR	VAR, HOM, CON, DIS, ENT	9 × 9	Li, Lu, et al. (2011)
ALOS PALSAR	HH and HV	VAR, HOM, CON, DIS, ENT, SEM	5 × 5, 9 × 9, 15 × 15, 19 × 19, 25 × 25, 31 × 31	Li, Lu, Moran, Dutra, et al. (2012)
SPOT HRG	Panchromatic band	MEA, VAR, HOM, CON, DIS, ENT, SEM, COR	3 × 3, 5 × 5, 7 × 7, 9 × 9, 11 × 11, 15 × 15, 19 × 19, 25 × 25, 31 × 31	Lu et al. (2008)
QuickBird	Red and NIR	MEA, HOM, DIS, SEM	9 × 9, 15 × 15, 21 × 21	Lu, Hetrick, and Moran (2010)

Note: See Table 2 for explanations of texture measures.

user's and producer's accuracies are commonly used to assess the accuracy of individual classes, but sometimes this may lead to mistakes because, for some land-cover classes, the producer's accuracy may be high but the user's accuracy may be low, or vice versa. In order to avoid this problem and provide comparative analysis of classification results among different scenarios using the textural images from different sensor data, the accuracy for an individual land-cover class (AILC) is defined as:

$$\mathrm{AILC} = \frac{(\mathrm{PA}) \times (\mathrm{UA})}{[(\mathrm{PA}) + (\mathrm{UA})]/2}, \tag{2}$$

and overall accuracy based on AILC (OA_AILC) is defined as:

$$\mathrm{OA\_AILC} = \frac{1}{n}\sum_{i=1}^{n} \mathrm{AILC}_i, \tag{3}$$

where UA and PA are user's and producer's accuracies, n is the number of land-cover classes, and AILC_i represents the ith land-cover type. Therefore, we can easily evaluate the individual land-cover classification accuracy using AILC and compare the performances of different classification results using OA_AILC.

4. Results and discussion

4.1. Analysis of the best combination of textural images

Based on the analysis of BTC for potential textural images, the best combination of textural images for each satellite image was obtained, and the results are summarized in Table 4. Although the best combination of textural images for different sensor data varies, the results in Table 4 indeed provide some important information about the selection of texture measures and window sizes. For example, a window size of 9 × 9 pixels is suitable for optical sensor data, but a large window size of 25 × 25 pixels is needed for ALOS PALSAR data. A large window size for ALOS PALSAR data may be beneficial to further reduce the speckle problem (Li, Lu, Moran, Dutra, et al. 2012). Concerning the selection of texture measures, dissimilarity seems good for optical sensor data, and contrast and second moment are suitable for ALOS PALSAR data. Table 4 also indicates that the best texture combinations vary, depending on the specific sensor, implying the necessity to identify the optimal texture combination corresponding to a specific data set. The different characteristics of various sensor data and different biophysical environments of study

Table 4. Identified best combinations used in land-cover classification procedures.

Sensor	Best texture combination	Band	Texture measure(s)	Window size(s)
Landsat 5 TM	Red-DIS9, NIR-DIS9	Red, NIR	DIS	9 × 9
ALOS PALSAR L-band	HH-SEM25, HH-CON31	HH	SEM, CON	25 × 25, 31 × 31
	HV-CON25, HV-SEM19	HV	CON, SEM	25 × 25, 19 × 19
SPOT 5 HRG	PAN-ENT9, PAN-DIS15	PAN	ENT, DIS	9 × 9, 15 × 15
QuickBird	Red-DIS9, Red-MEA9	Red	DIS, MEA	9 × 9

Note: See Table 2 for explanations of texture measures.

areas require analysts to identify specific texture images for each situation. This produces a challenge for quickly identifying the best textural images for a specific study.

Figure 3 provides a comparison between a Landsat TM NIR image and two corresponding textural images, implying different characteristics in reflecting land covers. The textural image based on the red band (i.e. Landsat TM band 3, shown in Figure 3(*b*)) highlights non-vegetation information such as urban buildings and roads, and the textural image based on the TM NIR image (Figure 3(*c*)) highlights the difference between vegetation and non-vegetation types. Figure 4 illustrates the textural images that are calculated using different measures but the same window size (9 × 9) using the SPOT HRG panchromatic band, implying their different capabilities in extracting land surface features. For example, the textural images using Variance (Figure 4(*b*)), Contrast (Figure 4(*d*)), and Dissimilarity (Figure 4(*e*)) highlight similar linear features such as roads, and the textural image using Entropy (Figure 4(*f*)) further enhances the finer linear features. On the other hand, the texture image produced using the second moment has richer information than that obtained using the correlation coefficient (Figure 4(*g*) vs. Figure 4(*f*)). Figure 4 also indicates the high correlations that exist between some textural images because they represent similar information such as Figures 4(*d*) and (*e*). Figure 5 compares ALOS PALSAR HH and HV, and their two corresponding texture images, indicating their complementary information. Comparing them with Figure 3 for the same study area, the textural images from ALOS PALSAR can be seen to contain much less information than the Landsat TM optical images, implying that the ALOS PALSAR-based textural images have less capability for representing land-cover surface characteristics. Figure 6 provides a comparison of textural images using the same texture measure but different window sizes, implying the importance of using an optimal window size in extracting land-cover features. Large window sizes produce blurred boundaries between land-cover types and enlarge linear features such as roads, resulting in poor classification for some land-cover types such as roads and small patch classes with high spectral signatures.

4.2. *Analysis of land-cover classification results*

Landsat TM multispectral images indeed provide much better classification accuracy than pure textural images, as shown in Table 5. However, incorporation of spectral and textural images improved overall classification accuracy by 3%. Considering individual classes,

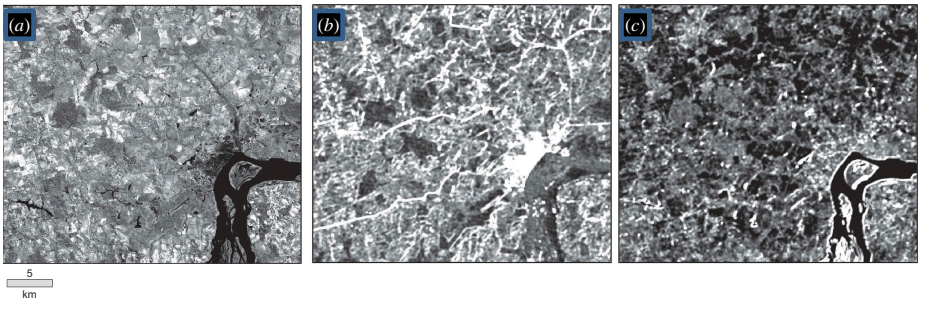

Figure 3. A comparison of (*a*) Landsat TM band 4 (NIR), (*b*) textural image obtained using the measure 'dissimilarity' on band 3 (red) and a window size of 9 × 9 pixels, and (*c*) textural image obtained using dissimilarity on band 4 (NIR) and window size of 9 × 9 pixels at Altamira.

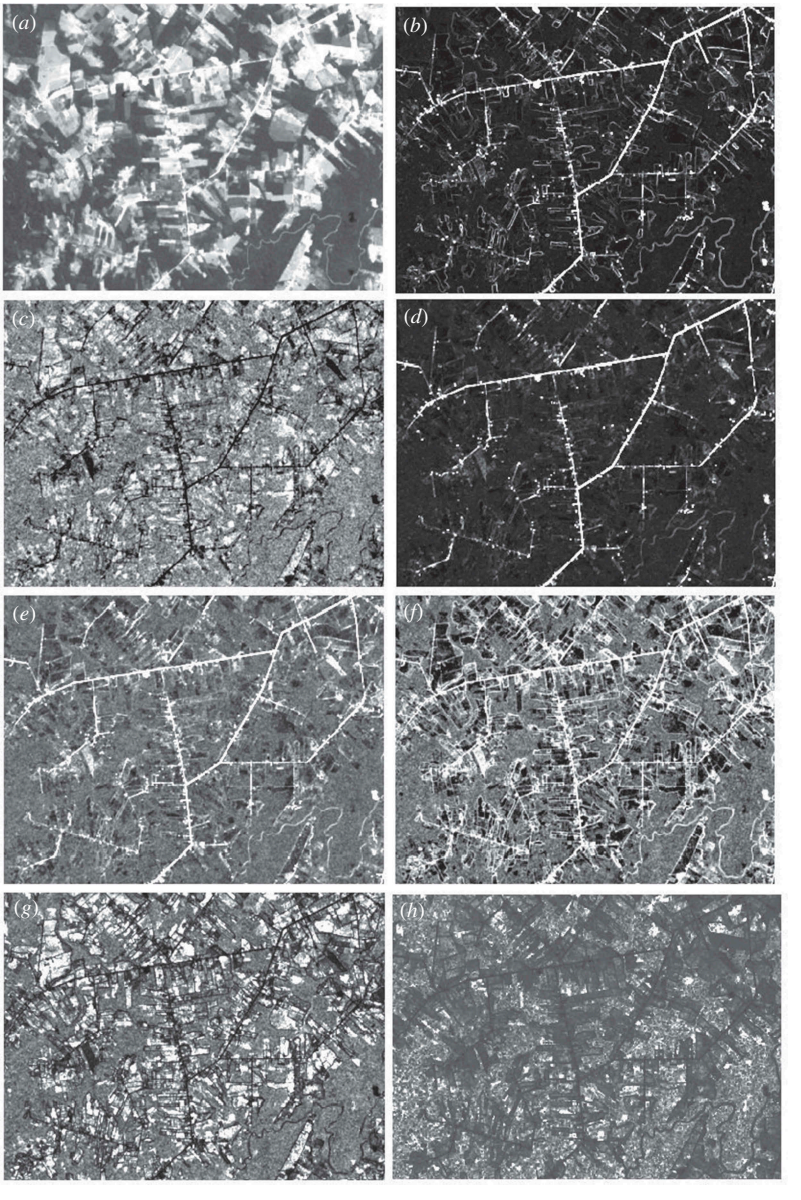

Figure 4. Textural images obtained from the SPOT panchromatic band based on different texture measures but the same window size (9 × 9) for Machadinho d'Oeste; (*a*), (*b*), (*c*), (*d*), (*e*), (*f*), (*g*), and (*h*) represent the textural images calculated using mean, variance, homogeneity, contrast, dissimilarity, entropy, second moment, and correlation coefficient, respectively.

most land-cover classes, except upland forest and urban, have better classification results using spectral signatures than using textural images. Yet, a combination of spectral and textural images improved the accuracy of most land-cover types, except liana forest, initial secondary succession (SS1), and pasture, implying the important role of textural images in improving land-cover classification, but not for all land-cover types. When the overall

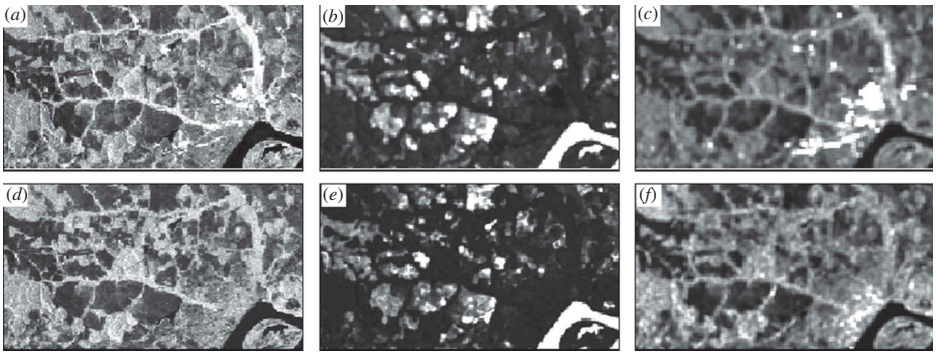

Figure 5. A comparison between ALOS PALSAR L-band HH and HV images and corresponding textural images of Altamira; (*a*), (*b*), and (*c*) are HH image and HH-derived SM25 and CON31 textural images; (*d*), (*e*), and (*f*) are HV image and HV-derived CON25 and SM19 textural images. (For definitions, see Table 4.).

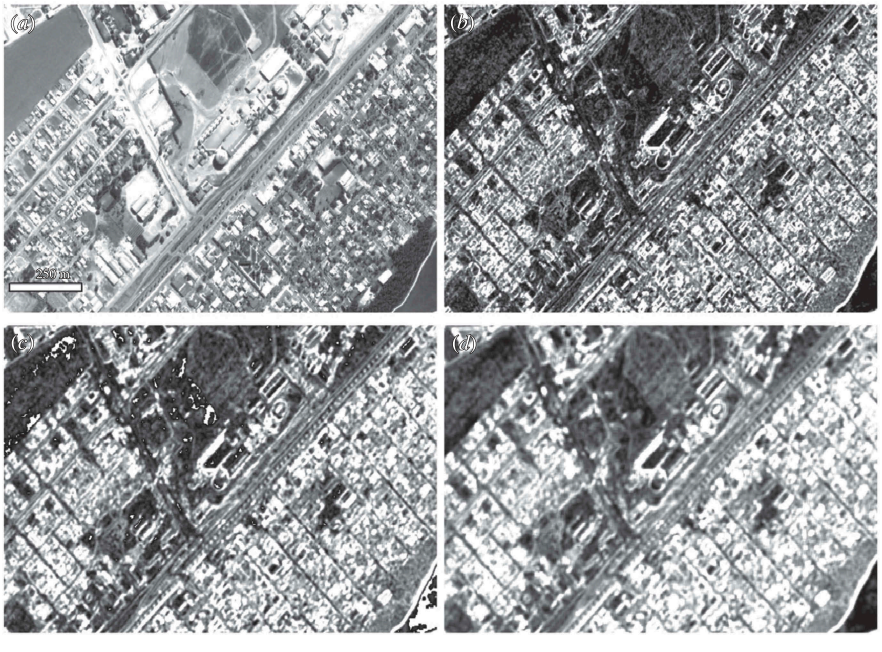

Figure 6. Comparison between textural images obtained from the QuickBird image of Lucas do Rio Verde; (*a*) red-band image; (*b*), (*c*), and (*d*) textural images derived using dissimilarity texture measure on the red-band images with window sizes of 9 × 9 pixels, 15 × 15 pixels, and 21 × 21 pixels, respectively.

accuracy is evaluated using OA_AILC, the accuracy improved by 5.2% from 76.6% to 81.8%.

Compared to the classification results for the Landsat TM image (see Table 5), ALOS PALSAR data provided lower classification accuracy for the same study area, as summarized in Table 6. ALOS PALSAR radiometric data can provide good

Table 5. Comparison of accuracy assessment results obtained using the Landsat TM image of Altamira.

	Spectral bands			Textural images			Combination		
Land-cover type	PA (%)	UA (%)	AILC (%)	PA (%)	UA (%)	AILC (%)	PA (%)	UA (%)	AILC (%)
Upland forest	37.0	95.2	53.2	61.1	61.1	61.2	66.7	78.3	72.0
Flooding forest	93.8	50.0	65.2	0.0	0.0	0.0	100.0	66.7	80.0
Liana forest	95.5	66.7	78.6	77.3	30.6	43.8	81.8	66.7	73.4
SS1	84.0	61.8	71.2	36.0	34.6	35.2	92.0	57.5	70.8
SS2	67.9	90.5	77.6	3.6	14.3	5.8	78.6	95.7	86.4
SS3	89.7	74.3	81.2	0.0	0.0	0.0	79.3	85.2	82.2
Pasture	83.3	94.8	88.6	54.6	51.4	53.0	75.8	96.2	84.8
Water	68.2	100.0	81.0	50.0	73.3	59.4	72.7	100.0	84.2
Wetland	53.9	100.0	70.0	0.0	0.0	0.0	69.2	100.0	81.8
Urban	100.0	71.1	83.2	100.0	81.8	90.0	100.0	79.4	88.6
Burned area	100.0	87.5	93.4	28.6	21.1	24.2	92.9	100.0	96.4
Overall accuracy (%)	77.2			45.9			80.2		
OA_AILC (%)			76.6			33.8			81.8

Note: SS1, SS2, and SS3 are initial, intermediate, and advanced successional stages of forest, respectively.

Table 6. Comparison of land-cover classification results based on different combinations of HH and HV polarizations, textural images, and their combinations for ALOS PALSAR L-band data of Altamira.

	Radiometric bands			Textural images			Combination		
Land-cover types	PA (%)	UA (%)	AILC (%)	PA (%)	UA (%)	AILC (%)	PA (%)	UA (%)	AILC (%)
Upland forest	27.3	30.0	28.6	12.1	80.0	21.0	51.5	39.5	44.8
Flooded forest	80.0	54.6	65.0	6.7	50.0	11.8	73.3	61.1	66.6
Liana forest	0.0	0.0	0.0	0.0	0.0	0.0	25.0	15.8	19.4
SS1	31.6	46.2	37.6	10.5	100.0	19.0	42.1	50.0	45.8
SS2	54.2	33.3	41.2	33.3	61.5	43.2	66.7	64.0	65.4
SS3	23.8	27.8	25.6	4.8	100.0	9.2	23.8	38.5	29.4
Agropasture	88.5	53.5	66.6	80.8	61.8	70.0	76.9	62.5	69.0
Water	95.8	100.0	97.8	87.5	91.3	89.4	83.3	95.2	88.8
Wetland	26.7	50.0	34.8	40.0	50.0	44.4	33.3	55.6	41.6
Urban	30.4	77.8	43.8	95.7	18.3	30.8	60.9	87.5	71.8
Overall accuracy (%)	48.1			40.6			56.1		
OA_AILC (%)			44.1			33.9			54.3

Note: HH, horizontal transmission and receipt of polarization; HV, horizontal transmission and vertical receipt of polarization; SS1, SS2, and SS3 are initial, intermediate, and advanced successional stages of forest, respectively.

accuracy only for flooded forest, agropasture, and water, and textural images provide reasonably good results for agropasture and water. Overall, textural images have less capability in land-cover classification than ALOS PALSAR radiometric data, but the combination of them did improve overall accuracy by 8%, from 48.1% to 56.1%, and OA_AILC by 10.2%. Because ALOS PALSAR data represent the roughness of land-cover surface, the similar roughness among upland forest, liana forest, and advanced secondary succession (SS3) result in poor separability among them. Yet, the ALOS PALSAR data can penetrate forest canopy to capture some information under the canopy, such as water in a flooded forest, thereby making ALOS PALSAR data capable of providing better classification performance for flooded forest in comparison with other forest types.

The higher spatial resolution of SPOT HRG data does not guarantee improvement in vegetation classification compared to Landsat images with 30 m spatial resolution; however, the study areas lack sound comparison because of the use of different vegetation classification systems and the presence of different biophysical environments. The combination of spectral and textural images improved overall classification accuracy by 5.5% when comparing only spectral signatures of the SPOT data. For individual classes, the combination improved classification of most land-cover types, especially for upland open forest and cultivated pastures (Table 7). When we compared the same pixel sizes of ALOS PALSAR and SPOT HRG images, textural images obtained from ALOS PALSAR data seem to play a more important role in improving land-cover classification than those from SPOT data.

For very-high-spatial-resolution QuickBird images, the land-cover classification in the urban–rural landscape cannot provide satisfactory results using only spectral signatures. The major problem is the shadows cast by buildings and tall trees, the spectral confusion between impervious surfaces, bare soils, and low-spectral objects such as water and shadow, and high spectral variation within the same land-cover types (Lu, Hetrick, and Moran 2010). Use of textural images can reduce some problems such as the spectral variation within the same land cover and the shadows. Therefore, the combination of spectral and textural images improved land-cover classification by 11.6% in overall accuracy or 13.4% in OA_AILC compared to using only QuickBird spectral signatures (Table 8). All land-cover classification accuracy is improved through incorporation of textural images into multispectral data, implying the importance of using textural images in high-spatial-resolution images.

4.3. Comparative analysis of overall classification performance among different types of sensor data

A summary of overall classification assessment results is provided in Table 9, indicating that there are significantly different roles for textural images obtained from different sensors in improving land-cover classification. Comparing Landsat TM 30 m optical data to 10 m SPOT multispectral data and the 0.6 m fused QuickBird multispectral image, the OA_AILC increased from 5.2% to 13.4%, suggesting that there is an important role for textural images in improving land-cover classification as the spatial resolution of the optical sensor data increases. Compared to optical sensor data, incorporation of textural images into ALOS PALSAR data is especially valuable in improving classification. For ALOS PALSAR and SPOT HRG data with the same pixel size, the OA_AILC for the ALOS PALSAR data improved by 10.2% compared to the 6.6% improvement in OA_AILC for the SPOT data, implying the important role of texture features in reducing speckle and also the heterogeneity inherent within the same land-cover type in ALOS PALSAR data.

Table 7. Comparison of classification results for different combinations of SPOT HRG multispectral and textural images obtained from the panchromatic band for Machadinho d'Oeste.

	Spectral bands			Combination		
Land-cover type	PA (%)	UA (%)	AILC (%)	PA (%)	UA (%)	AILC (%)
Upland dense forest	62.5	92.6	74.6	67.5	93.1	78.2
Upland open forest	58.3	58.3	58.4	100.0	75.0	85.8
Flooded forest	75.0	42.9	54.6	75.0	46.2	57.2
SS3	66.7	30.0	41.4	66.7	35.3	46.2
SS2	47.2	38.6	42.4	61.1	43.1	50.6
SS1	62.0	63.3	62.6	54.0	62.8	58.0
Dirty pasture	63.2	49.0	55.2	71.1	50.9	59.4
Cultivated pasture	66.0	86.8	75.0	84.0	95.5	89.4
Agroforestry	50.8	76.2	61.0	46.0	85.3	59.8
Overall accuracy (%)	59.2			64.7		
OA_AILC (%)			58.4			65.0

Note: SS3, SS2, and SS1 are advanced, intermediate, and initial successional stages of forest, respectively.

Table 8. A comparison of accuracy assessment results obtained using QuickBird images of Lucas do Rio Verde.

	Spectral bands			Combination		
Land-cover type	PA (%)	UA (%)	AILC (%)	PA (%)	UA (%)	AILC (%)
Forest	92.5	71.0	80.4	95.1	89.2	92.0
Impervious	95.1	76.5	84.8	90.9	85.1	88.0
Pasture/grass	75.0	62.3	68.0	74.5	77.8	76.0
Water	71.0	100.0	83.0	80.0	100.0	88.8
Wetland	31.0	52.9	39.2	88.9	72.7	80.0
Bare land	69.7	82.1	75.4	87.1	93.1	90.0
Fields	75.4	86.7	80.6	89.9	91.2	90.6
Overall accuracy (%)	75.7			87.3		
OA_AILC (%)			73.1			86.5

Table 9. Summary of overall classification accuracies for data from different sensors.

		OA_AILC (%)		
Data type	Pixel size (m)	Original bands	Combination	Improvement in accuracy (%)
Landsat TM	30	76.6	81.8	5.2
ALOS PALSAR	10	44.1	54.3	10.2
SPOT HRG	10	58.4	65.0	6.6
QuickBird	0.6	73.1	86.5	13.4

Although the importance of using textural images in improving land-cover classification is recognized, the above analysis shows the complexity and challenges inherent in identifying suitable textural images for a specific study as these depend on the specific sensor data used and the characteristics of the landscapes under investigation. This implies that it is still difficult to obtain general guidelines that can be used to support the automatic selection of textural images in a particular study, because the performance of textural images relies on the complex combination of texture measures, the specific image data used, window size, and the land-cover types present. Overall, incorporation of textural images into spectral or radiometric images is beneficial to improving land-cover classification, but not for all land-cover types. Use of textures may improve the classification of some land-cover types such as primary forest due to reduction of spectral heterogeneity but may reduce the accuracy of the classification of other cover types such as secondary forest due to its relatively small patch size. More research is needed to conduct a comparative analysis between images with different spatial resolutions covering the same study areas. This could be done, for example, for vegetation-dominated mountainous regions to examine how to select suitable textures for improving vegetation classification or for landscapes dominated by urban land use to help understand which textures provide better performance for improving urban land-cover classification.

5. Summary

This research shows the importance of textural images in improving land-cover classification. The capability of textural features to reduce speckle/noise and to address the heterogeneity inherent within the same land-cover types makes this especially important for land-cover classification using ALOS PALSAR data and the very-high-spatial-resolution QuickBird imagery. Because of the high correlation between some textural images, it is important to identify the textural images that have good separability for land-cover types but low correlation between the textural images. Not all textural images are needed. A combination of two textural images is sufficient for land-cover classification, but pure textural images cannot provide good land-cover classification. Overall, textural images have less capability for distinguishing between land-cover types than spectral signatures, especially for medium spatial resolution images, but the textural images become more useful as spatial resolution increases. The OA_AILC can be improved from 5.2% to 13.4% as the spatial resolution decreases from 30 m to 0.6 m. More research is needed on the development of new methods to conduct automatic selection of optimal combinations of textural images for a specific study, such as for land-cover classification.

Acknowledgements

Luciano Dutra thanks the Japan Aerospace Exploration Agency (AO 108) Science Programme for providing the ALOS (Advanced Land Observing Satellite) PALSAR (Phased Array type L-band Synthetic Aperture Radar) data.

Funding

The authors acknowledge the support from the Zhejiang A&F University's Research and Development Fund for the talent start-up project (2013FR052), Zhejiang Provincial Key Laboratory of Carbon Cycling in Forest Ecosystems and Carbon Sequestration at Zhejiang A&F University, and the Center for Global Change and Earth Observations at Michigan State University.

References

Agüera, F., F. J. Aguilar, and M. Aguilar. 2008. "Using Texture Analysis to Improve Per-Pixel Classification of Very High Resolution Images for Mapping Plastic Greenhouses." *ISPRS Journal of Photogrammetry and Remote Sensing* 63 (6): 635–646. doi:10.1016/j.isprsjprs.2008.03.003.

Bannari, A., D. Morin, F. Bonn, and A. R. Huete. 1995. "A Review of Vegetation Indices." *Remote Sensing Reviews* 13: 95–120. doi:10.1080/02757259509532298.

Chander, G., B. L. Markham, and D. L. Helder. 2009. "Summary of Current Radiometric Calibration Coefficients for Landsat MSS, TM, ETM+, and EO-1 ALI Sensors." *Remote Sensing of Environment* 113: 893–903. doi:10.1016/j.rse.2009.01.007.

Chavez, P. S. Jr. 1996. "Image-Based Atmospheric Corrections: Revisited and Improved." *Photogrammetric Engineering and Remote Sensing* 62: 1025–1036.

Chen, D., D. A. Stow, and P. Gong. 2004. "Examining the Effect of Spatial Resolution and Texture Window Size on Classification Accuracy: An Urban Environment Case." *International Journal of Remote Sensing* 25 (11): 2177–2192. doi:10.1080/01431160310001618464.

Coburn, C. A., and A. C. B. Roberts. 2004. "A Multiscale Texture Analysis Procedure for Improved Forest Stand Classification." *International Journal of Remote Sensing* 25 (20): 4287–4308. doi:10.1080/0143116042000192367.

Congalton, R. G. 1991. "A Review of Assessing the Accuracy of Classifications of Remotely Sensed Data." *Remote Sensing of Environment* 37 (1): 35–46. doi:10.1016/0034-4257(91)90048-B.

Congalton, R. G., and K. Green. 2008. *Assessing the Accuracy of Remotely Sensed Data: Principles and Practices*. 2nd ed. Boca Raton, FL: CRC Press.

Culbert, P. D., V. C. Radeloff, V. St-Louis, C. H. Flather, C. D. Rittenhouse, T. P. Albright, and A. M. Pidgeon. 2012. "Modeling Broad-Scale Patterns of Avian Species Richness across the Midwestern United States with Measures of Satellite Image Texture." *Remote Sensing of Environment* 118: 140–150. doi:10.1016/j.rse.2011.11.004.

Cutler, M. E. J., D. S. Boyd, G. M. Foody, and A. Vetrivel. 2012. "Estimating Tropical Forest Biomass with a Combination of SAR Image Texture and Landsat TM Data: An Assessment of Predictions Between Regions." *ISPRS Journal of Photogrammetry and Remote Sensing* 70: 66–77. doi:10.1016/j.isprsjprs.2012.03.011.

Dutra, L. V., and N. D. A. Mascarenhas. 1984. "Some Experiments with Spatial Feature Extraction Methods in Multispectral Classifications." *International Journal of Remote Sensing* 5 (2): 303–313. doi:10.1080/01431168408948810.

Foody, G. M. 2002. "Status of Land Cover Classification Accuracy Assessment." *Remote Sensing of Environment* 80 (1): 185–201. doi:10.1016/S0034-4257(01)00295-4.

Foody, G. M. 2009. "Classification Accuracy Comparison: Hypothesis Tests and the Use of Confidence Intervals in Evaluations of Difference, Equivalence and Non-Inferiority." *Remote Sensing of Environment* 113 (8): 1658–1663. doi:10.1016/j.rse.2009.03.014.

Haralick, R. M., K. Shanmugam, and I. Dinstein. 1973. "Textural Features for Image Classification." *IEEE Transactions on Systems, Manual and Cybernetics* 3 (6): 610–621. doi:10.1109/TSMC.1973.4309314.

Herold, M., X. Liu, and K. C. Clarke. 2003. "Spatial Metrics and Image Texture for Mapping Urban Land Use." *Photogrammetric Engineering & Remote Sensing* 69 (9): 991–1001. doi:10.14358/PERS.69.9.991.

Jin, H., P. Li, T. Cheng, and B. Song. 2012. "Land Cover Classification Using CHRIS/PROBA Images and Multi-Temporal Texture." *International Journal of Remote Sensing* 33 (1): 101–119. doi:10.1080/01431161.2011.584077.

Johansen, K., N. C. Coops, S. E. Gergel, and Y. Stange. 2007. "Application of High Spatial Resolution Satellite Imagery for Riparian and Forest Ecosystem Classification." *Remote Sensing of Environment* 110 (1): 29–44. doi:10.1016/j.rse.2007.02.014.

Kayitakire, F., C. Hamel, and P. Defourny. 2006. "Retrieving Forest Structure Variables Based on Image Texture Analysis and IKONOS-2 Imagery." *Remote Sensing of Environment* 102 (3–4): 390–401. doi:10.1016/j.rse.2006.02.022.

Kourgli, A., M. Ouarzeddine, Y. Oukil, and A. Belhadj-Aissa. 2012. "Texture Modelling for Land Cover Classification of Fully Polarimetric SAR Images." *International Journal of Image and Data Fusion* 3 (2): 129–148. doi:10.1080/19479832.2010.551521.

Kuplich, T. M., P. J. Curran, and P. M. Atkinson. 2005. "Relating SAR Image Texture to the Biomass of Regenerating Tropical Forests." *International Journal of Remote Sensing* 26 (21): 4829–4854. doi:10.1080/01431160500239107.

Li, G., D. Lu, E. Moran, L. Dutra, and M. Batistella. 2012. "A Comparative Analysis of ALOS PALSAR L-Band and RADARSAT-2 C-Band Data for Land-Cover Classification in a Tropical Moist Region." *ISPRS Journal of Photogrammetry and Remote Sensing* 70: 26–38. doi:10.1016/j.isprsjprs.2012.03.010.

Li, G., D. Lu, E. Moran, and S. Hetrick. 2011. "Land-Cover Classification in a Moist Tropical Region of Brazil with Landsat Thematic Mapper Imagery." *International Journal of Remote Sensing* 32 (23). doi:10.1080/01431161.2010.532831.

Li, G., D. Lu, E. Moran, and S. J. S. Sant'Anna. 2012. "Comparative Analysis of Classification Algorithms and Multiple Sensor Data for Land Use/Land Cover Classification in the Brazilian Amazon." *Journal of Applied Remote Sensing* 6 (1): 061706. doi:10.1117/1.JRS.6.061706.

Li, Z., R. Hayward, Y. Liu, and R. Walker. 2011. "Spectral-Texture Feature Extraction Using Statistical Moments with Application to Object-Based Vegetation Species Classification." *International Journal of Image and Data Fusion* 2 (4): 347–361. doi:10.1080/19479832.2010.546372.

Lu, D., M. Batistella, E. Moran, and E. E. De Miranda. 2008. "A Comparative Study of Landsat TM and SPOT HRG Images for Vegetation Classification in the Brazilian Amazon." *Photogrammetric Engineering and Remote Sensing* 74 (3): 311–321. doi:10.14358/PERS.74.3.311.

Lu, D., Q. Chen, G. Wang, E. Moran, M. Batistella, M. Zhang, G. Vaglio Laurin, and D. Saah. 2012. "Aboveground Forest Biomass Estimation with Landsat and LiDAR Data and Uncertainty Analysis of the Estimates." *International Journal of Forestry Research* 2012: 1–16. doi:10.1155/2012/436537.

Lu, D., S. Hetrick, and E. Moran. 2010. "Land Cover Classification in a Complex Urban-Rural Landscape with QuickBird Imagery." *Photogrammetric Engineering and Remote Sensing* 76 (10): 1159–1168. doi:10.14358/PERS.76.10.1159.

Lu, D., P. Mausel, M. Batistella, and E. Moran. 2004. "Comparison of Land-Cover Classification Methods in the Brazilian Amazon Basin." *Photogrammetric Engineering and Remote Sensing* 70 (6): 723–731. doi:10.14358/PERS.70.6.723.

Lu, D., and Q. Weng. 2007. "A Survey of Image Classification Methods and Techniques for Improving Classification Performance." *International Journal of Remote Sensing* 28 (5): 823–870. doi:10.1080/01431160600746456.

Marceau, D. J., P. J. Howarth, J. M. Dubois, and D. J. Gratton. 1990. "Evaluation of the Grey-Level Co-Occurrence Matrix Method for Land-Cover Classification Using SPOT Imagery." *IEEE Transactions on Geoscience and Remote Sensing* 28 (4): 513–519. doi:10.1109/TGRS.1990.572937.

Marpu, P. R., M. Pedergnana, M. D. Mura, S. Peeters, J. A. Benediktsson, and L. Bruzzone. 2012. "Classification of Hyperspectral Data Using Extended Attribute Profiles Based on Supervised and Unsupervised Feature Extraction Techniques." *International Journal of Image and Data Fusion* 3 (3): 269–298. doi:10.1080/19479832.2012.702687.

McDonald, A. J., F. M. Gemmell, and P. E. Lewis. 1998. "Investigation of the Utility of Spectral Vegetation Indices for Determining Information on Coniferous Forests." *Remote Sensing of Environment* 66: 250–272. doi:10.1016/S0034-4257(98)00057-1.

Pathak, V., and O. Dikshit. 2010. "A New Approach for Finding an Appropriate Combination of Texture Parameters for Classification." *Geocarto International* 25 (4): 295–313. doi:10.1080/10106040903576195.

Rodriguez-Galiano, V. F., M. Chica-Olmo, F. Abarca-Hernandez, P. M. Atkinson, and C. Jeganathan. 2012. "Random Forest Classification of Mediterranean Land Cover Using Multi-Seasonal Imagery and Multi-Seasonal Texture." *Remote Sensing of Environment* 121: 93–107. doi:10.1016/j.rse.2011.12.003.

Sarker, L. R., and J. E. Nichol. 2011. "Improved Forest Biomass Estimates Using ALOS AVNIR-2 Texture Indices." *Remote Sensing of Environment* 115: 968–977. doi:10.1016/j.rse.2010.11.010.

Seetharaman, K., and N. Palanivel. 2013. "Texture Characterization, Representation, Description, and Classification Based on Full Range Gaussian Markov Random Field Model with Bayesian Approach." *International Journal of Image and Data Fusion* 4 (4): 342–362. doi:10.1080/19479832.2013.804007.

Su, W., J. Li, Y. Chen, Z. Liu, J. Zhang, T. M. Low, I. Suppiah, and S. A. M. Hashim. 2008. "Textural and Local Spatial Statistics for the Object-Oriented Classification of Urban Areas

Using High Resolution Imagery." *International Journal of Remote Sensing* 29 (11): 3105–3117. doi:10.1080/01431160701469016.

Viedma, O., I. Torres, B. Pérez, and J. M. Moreno. 2012. "Modeling Plant Species Richness Using Reflectance and Texture Data Derived from QuickBird in a Recently Burned Area of Central Spain." *Remote Sensing of Environment* 119: 208–221. doi:10.1016/j.rse.2011.12.024.

Wang, L., W. P. Sousa, P. Gong, and G. S. Biging. 2004. "Comparison of IKONOS and QuickBird Images for Mapping Mangrove Species on the Caribbean Coast of Panama." *Remote Sensing of Environment* 91 (3–4): 432–440. doi:10.1016/j.rse.2004.04.005.

Wood, E. M., A. M. Pidgeon, V. C. Radeloff, and N. S. Keuler. 2012. "Image Texture as a Remotely Sensed Measure of Vegetation Structure." *Remote Sensing of Environment* 121: 516–526. doi:10.1016/j.rse.2012.01.003.

Yu, J., Q. Yan, Z. Zhang, H. Ke, Z. Zhao, and W. Wang. 2012. "Unsupervised Classification of Polarimetric Synthetic Aperture Radar Images Using Kernel Fuzzy C-Means Clustering." *International Journal of Image and Data Fusion* 3 (4): 319–332. doi:10.1080/19479832.2012.668951.